

Article

On the Steady-State Flow and Yielding Behaviour of Lubricating Greases

Miguel A. Delgado *, Sebastien Secouard, Concepción Valencia and José M. Franco * 

Pro2TecS-Chemical Process and Product Technology Research Center, Universidad de Huelva, Campus El Carmen, 21071 Huelva, Spain; sebastien.secouard@fresenius-kabi.com (S.S.); barragan@uhu.es (C.V.)

* Correspondence: miguel.delgado@diq.uhu.es (M.A.D.); franco@uhu.es (J.M.F.); Tel.: +34-959-219-865 (M.A.D.); +34-959-219-995 (J.M.F.)

Received: 6 December 2018; Accepted: 4 January 2019; Published: 9 January 2019



Abstract: Practical steady-state flow curves were obtained from different rheological tests and protocols for five lubricating greases, containing thickeners of a rather different nature, i.e., aluminum complex, lithium, lithium complex, and calcium complex soaps and polyurea. The experimental results demonstrated the difficulty to reach “real” steady-state flow conditions for these colloidal suspensions as a consequence of the strong time dependence and marked yielding behavior in a wide range of shear rates, resulting in flow instabilities such as shear banding and fracture. In order to better understand these phenomena, transient flow experiments, at constant shear rates, and creep tests, at constant shear stresses, were also carried out using controlled-strain and controlled-stress rheometers, respectively. The main objective of this work was to study the steady-state flow behaviour of lubricating greases, analyzing how the microstructural characteristics may affect the yielding flow behaviour.

Keywords: lubricating grease; rheology; steady-state and transient flow; microstructure

1. Introduction

Lubricating greases are generally highly structured suspensions consisting of a thickener, usually a metal soap such as lithium, calcium, sodium, barium, or aluminum, dispersed in mineral or synthetic oils. In addition, lubricating greases usually contain some performance additives [1–3]. Thickener molecules combine to form tridimensional networks consisting of fibers, small spheres, rods, or platelets in which the oil is trapped, conferring the appropriate rheological and tribological behaviour to the grease. The main purpose of the thickener is to prevent the loss of lubricant under operating conditions, providing gel-like characteristics to the grease, despite this evidently implying a considerable resistance to the flow of these materials [2,4,5].

Special attention has been paid to the steady-state flow behaviour of lubricating greases because of the complex strain response to stress and the time-dependent behaviour exhibited [3–9]. It is accepted that lubricating greases are yielding materials, characterized by a discontinuity in the flow curve, particularly in the yielding stress range, where the deformation process is characterized by a sudden drop in viscosity when the shear stress slightly increases. The existence of three different regions in the viscous flow curve of lubricating greases has been previously discussed [6–10]: firstly, a tendency to reach a limiting viscosity, at very low stress values; secondly, a dramatic drop in viscosity; and finally, a tendency to reach a constant high-shear stress-limiting viscosity. The appropriate characterization of this flow behaviour has an evident practical importance, above all in relation to average life-time, resistance under operating conditions, and pumpability [2]. Indeed, this characteristic flow behaviour allows the “practical” yield stress value to be determined, which plays an important role in the design of automatic grease centralized pumping and distribution systems [5].

Very recently, different studies have pointed out the importance of the flow behavior in the correct evaluation of the fluid dynamics of greases in practical situations, for instance, by performing numerical simulations. In this sense, numerical simulations applying computational fluid dynamics (CFD) procedures or Runge-Kutta methods have been performed to predict the particle motion/migration in pockets between two-rotating cylinders with different restriction geometries [11,12], the grease flow in journal bearings as a function of surface texture [13], the dynamics of greases in tapered roller bearings [14], or the laminar flow in rectangular cross section channels [15], among other practical situations. Additionally, the dynamics of greases was experimentally studied in both a labyrinth seal geometry [16] and concentric cylinder configurations with a rotating shaft to simulate the grease flow in a double restriction seal geometry [17] using the microparticle image velocimetry technique. In most of these studies, the relevance of the yielding flow behavior, mainly approached by the Herschel-Bulkley model; the plastic viscosity; or the shear-thinning character of greases was emphasized.

In this regard, great efforts have been made to correctly determine the yield stress value in greases [18,19]. Thus, in order to get reproducible and accurate results, it is necessary to conveniently define all test conditions since the flow curve data and the yield stress values may be widely dependent on them. Although it is worth mentioning that some controversy about the concept of yielding flow and associated experimental difficulties has been traditionally found in the literature [20–22], it is obvious that the yield stress is a parameter commonly used in the industry because of the importance of knowing the stress-time relationship to predict the effective flow conditions [23].

Several investigations on the rheological properties of lubricating greases have dealt with the application of pre-shearing conditions to simplify and accelerate the consecution of the steady-state flow [4,5]. The application of pre-shearing results in both the absence of stress overshoot and a relatively rapid achievement of the steady-state in transient experiments. However, this procedure leads to significant microstructural changes that affect the original rigidity of the network formed by the thickener. Thus, the ionic and van der Waals forces that contribute to the viscoelasticity of this network are highly affected by pre-shearing, also dramatically influencing the entanglements among the structural units (fibers, rods, platelets, . . .) that make up the structural skeleton.

This paper attempts to describe and understand the “real” steady-state flow behaviour of greases without applying pre-shearing conditions. The main objective is to elucidate the effect of the time scale and shear protocol on the consecution of the steady-state flow conditions for a variety of the most commonly used types of lubricating greases.

2. Materials and Methods

2.1. Materials

Lubricating greases were kindly supplied by Total France (Lyon, France). They consist of mineral oils and different metal soaps or polyurea thickeners. Some relevant physical properties provided by the manufacturer are presented in Table 1. All studied greases have an NLGI 2 grade, except the calcium complex soap-based formulation, which is an NLGI 1 grade grease.

Table 1. Lubricating grease properties.

Soap	Oil Viscosity at 40 °C (cP)	NLGI Grade	Drop Point (°C)
Aluminum Complex	130	2	>250
Lithium	150	2	>150
Lithium Complex	160	2	>250
Calcium Complex	150	1	>250
Polyurea	110	2	>240

2.2. Rheological Characterization

The rheological characterization of this group of greases was carried out with both a RS-150 (ThermoHaake, Karlsruhe, Germany) controlled-stress rheometer, and an ARES (Rheometrics Scientific, Leatherhead, UK) controlled-strain rheometer. All tests were performed using serrated plate–plate geometries (35 mm in controlled-stress, 25 mm in controlled-strain; 1mm gap, 0.4 relative roughness) in order to prevent the wall slip effects typically found in these materials [10]. No gap influence was detected when performing tests with different plate-plate gaps (0.5–3 mm), thus confirming the absence of wall slip. All measurements were conducted at 25 °C, following the same recent thermal and mechanical history, i.e., 30 min resting time at the selected temperature, and replicated at least three times using new un-sheared samples.

2.2.1. Stepped Shear Rate and Shear Stress Ramps

Upward stepped ramps of shear rates and shear stresses traditionally employed to obtain steady-state flow curves were applied using both controlled-stress, in a 10–3000 Pa range of shear stress, and controlled-strain, in a 0.0125–100 s^{−1} range of shear rate, rheometers. Each point within the flow curve was acquired after shearing for 3 min in each step. This curve will be called the “practical” steady-state flow curve in the text.

2.2.2. Transient Experiments at Constant Shear Rate

Stress-growth experiments were performed, at 25 °C, in the controlled-strain rheometer at different constant shear rates (0.0125, 0.1, and 1 s^{−1}). The evolution of shear stress with time was monitored until a steady state was reached. However, some experiments, especially at 1 s^{−1}, were eventually stopped before a steady state was reached when fracture and/or partial expelling of the sample was detected.

2.2.3. Creep Tests

Different constant shear stresses were applied to grease samples, using a controlled-stress rheometer, and the corresponding shear rate was measured for a period of time. These creep experiments were carried out between 100 and 1000 Pa, depending on the consistency of the lubricating grease.

2.2.4. SAOS Experiments

In addition, small-amplitude oscillatory shear (SAOS) tests, inside the linear viscoelasticity range, were carried out in a frequency range between 0.01 and 100 rad/s, using a plate-plate geometry (35 mm diameter, 1 mm gap) in the controlled stress rheometer. Stress sweep tests, at 1 Hz, were previously performed on each sample to determine the linear viscoelasticity region.

2.3. Atomic Force Microscopy

The microstructural characterization of greases was carried out by means of atomic force microscopy (AFM) using a multimode apparatus connected to a Nanoscope-IV scanning probe microscope controller (Digital Instruments, Veeco Metrology Group Inc., Santa Barbara, CA, USA). All images were acquired in the tapping mode using Veeco Nanoprobe™ tips.

3. Results

3.1. Linear Viscoelastic Response and Microstructure

Figure 1 shows the mechanical spectra, in the linear viscoelasticity range, for the different lubricating greases studied. These mechanical spectra are qualitatively similar to those shown by other particle gels [24], supporting the idea that lubricating greases are highly structured systems, as has

also been detected by AFM microscopy (Figure 2). Some useful information about the microstructural network of these greases may be extracted from small-amplitude oscillatory shear measurements.

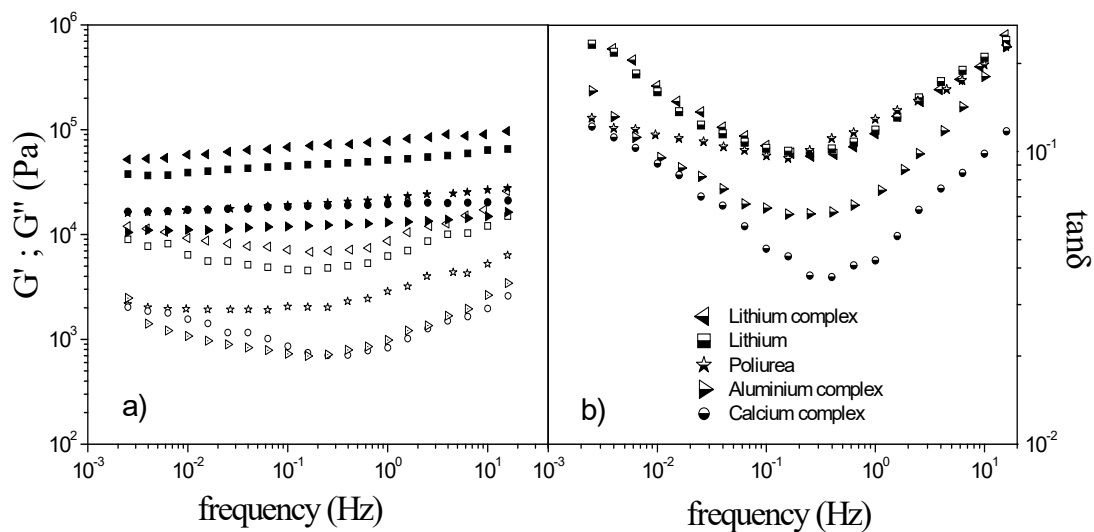


Figure 1. Frequency dependence of the storage and loss moduli (a) and $\tan \delta$ (b), in the linear viscoelasticity region, for the five lubricating greases studied (filled symbols, G' ; empty symbol, G'').

As typically found in commercial lubricating greases [25], all samples studied show values of the storage modulus (G') around one decade higher than those measured for the loss modulus (G''), as well as a minimum in G'' at intermediate frequencies. However, a much softer evolution was found for the polyurea-based grease, with almost constant values of G'' within the frequency range of around 10^{-3} – 10^{-1} Hz, and a gradual increase afterwards. On the other hand, very similar values of the loss tangent ($\tan \delta$) were obtained in most cases, with slightly lower values for the lithium and especially the complex calcium greases. In general, this viscoelastic behaviour is the result of both interparticle and thickener-oil interactions [7,26].

Although most of the samples studied are NLGI grade 2 greases (except the calcium complex soap-based grease), significant differences among them have been found from both viscoelastic and microstructural points of view. As can be observed in Figure 2, grease microstructures are very different, depending on the type of thickener, which determines the rheological behaviour of these lubricating greases. While most of the greases show a high density of soap particles in the form of small or long interconnected fibers, the calcium complex grease (Figure 2d) discloses a number of polydisperse large aggregates. Consequently, it may be assumed that this microstructure can exhibit a certain brittle character under shear, which can justify the relatively low values of $\tan \delta$ compared with the rest of the samples.

3.2. Stepped-Shear Rate and Stress Ramps: The “Practical” Steady-State Flow Curve

Figure 3 shows the viscous flow curves obtained from stepped-shear rate and stress ramps for the five grease samples studied. The shear stress versus shear rate curves were acquired by applying both the control stress (CS) and the controlled shear rate (CR) modes and plotted together, in a wide range of shear rates, to obtain the complete flow curves. In all cases, a strong shear rate dependence is appreciated. Initially, shear stress increases with shear rate up to around 10^{-3} s^{-1} , and shear stresses ranged from 500 Pa, for the lithium grease, to 1000 Pa, for the polyurea-based grease, which was only measurable in the CS mode. Then, the flow curves for the aluminum complex, lithium complex, and simple lithium greases exhibit several decades of almost constant values of shear stress between 10^{-3} and 10 s^{-1} , representative of the characteristic yielding flow behaviour of structured materials [6,10,27]. In addition, a slight non-monotonic evolution of the stress can be observed in this shear rate range (see, for instance, the lithium grease in Figure 3). However, calcium complex soap- and polyurea-based

greases clearly show a minimum in the shear stress vs. shear rate plots inside this range. These trends were only observed in the CR curves, whereas a sudden jump in the shear rate was observed in the CS curves in this shear rate range. Afterwards, above 10 s^{-1} , shear stress starts to increase again with shear rate, leading to coinciding CR and CS curves.

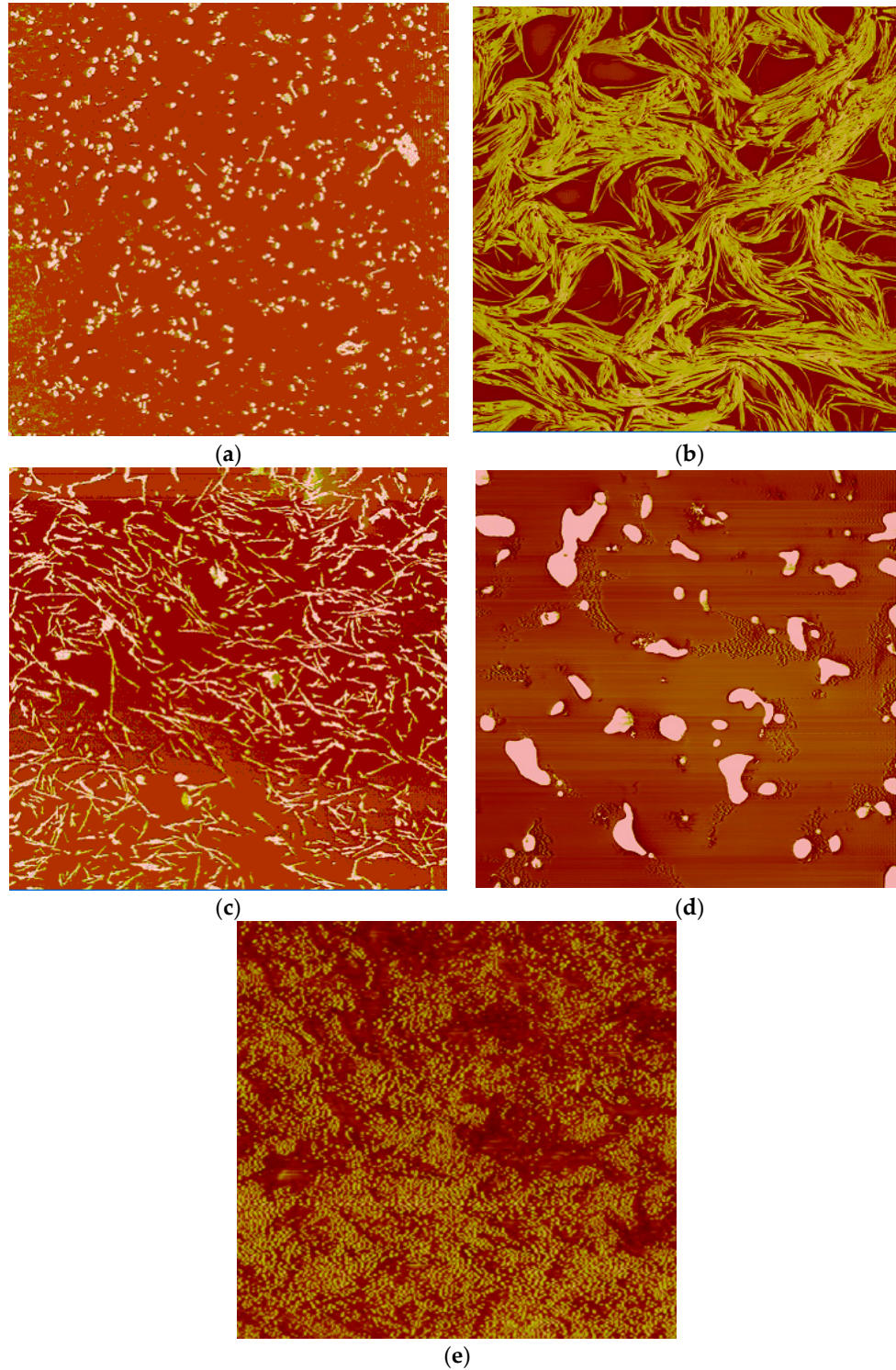


Figure 2. AFM photomicrographs for the five different lubricating greases studied (window size corresponds to $20 \mu\text{m}$): (a) aluminum complex, (b) lithium, (c) lithium complex, (d) calcium complex, and (e) polyurea * greases (* window size corresponds to $5 \mu\text{m}$).

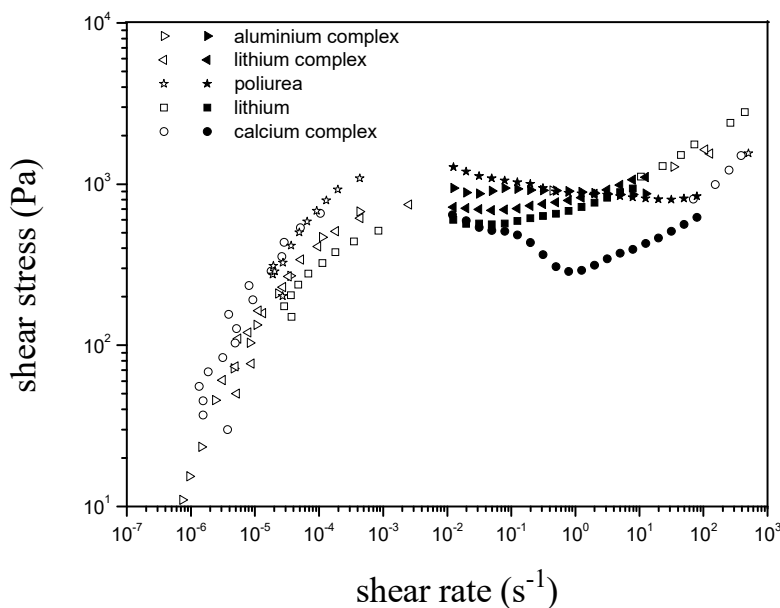


Figure 3. Stepped-stress and shear rate flow curves for the lubricating greases studied (filled symbols, CR curves; empty symbol, CS curves).

Traditionally, this behaviour has been attributed to a dynamically non-stable region and may be related to a non-homogeneous field of velocities during the viscometric flow of yielding materials, as, for instance, derived from wall depletion and shear banding phenomena, which can finally induce the fracture of the sample [28–31]. Thus, these experimental results, i.e., the jump in the stress in CS measurements and/or the minimum in stress eventually appearing in CR tests, have been explained by attending to the coexistence of three different shear rates at a given constant shear stress. In fact, only two possible steady flow regimes are possible since the other one corresponds to an unstable regime, which coincides with the part of the model in which the stress may decrease with shear rate [10]. Considering this model, a sudden transition from the low-shear rate to the high-shear rate regime was found in controlled-stress experiments and the fluid behaves like a typical yield stress fluid (Figure 3). This experimental flow curve has also been recently explained with simple mathematical arguments in the case of highly shear-thinning fluids, where the CR and CS shearing protocol modes play a decisive role in obtaining a minimum in the stress vs. shear rate plot [32]. This explanation does not need to be supported with the occurrence of flow instabilities as previously discussed, although the condition of a very pronounced shear-thinning behavior can easily promote such instabilities, since the apparent viscosity of the fluid will show huge variations along the gradient direction because of its enormous dependence on small shear stress variations. Nevertheless, as is discussed below, the non-consecution of steady conditions in stepped shear rate or stress ramps and the appearance of instabilities need to be additionally considered to explain the yielding behaviour of lubricating greases.

3.3. Transient Flow

In order to check the achievement of steady-state conditions in the stepped-shear rate and stress ramps, transient experiments at a constant shear rate or shear stress were performed for all the greases studied. Figure 4 shows the stress-growth curves obtained in transient experiments at constant shear rates of 0.0125, 0.1, and 1 s⁻¹. The evolution of the transient stress with time is similar to that observed for other thixotropic colloidal systems [20,33,34]. In all cases, a non-linear viscoelastic response was observed with two distinct regions: the first one between the onset of the transient test and the maximum shear stress, the so-called stress overshoot (τ_{max}); and the second one ranging between this maximum and the equilibrium or steady-state shear stress (τ_{eq}). The first part of these curves is mainly the result of the well-known viscoelastic response of greases, with elastic deformation of the prevailing

component. Thus, the stress overshoot has been related to the energy level that has to be applied on the grease to produce a significant structural breakdown, when the shear flow process begins to be predominant [35].

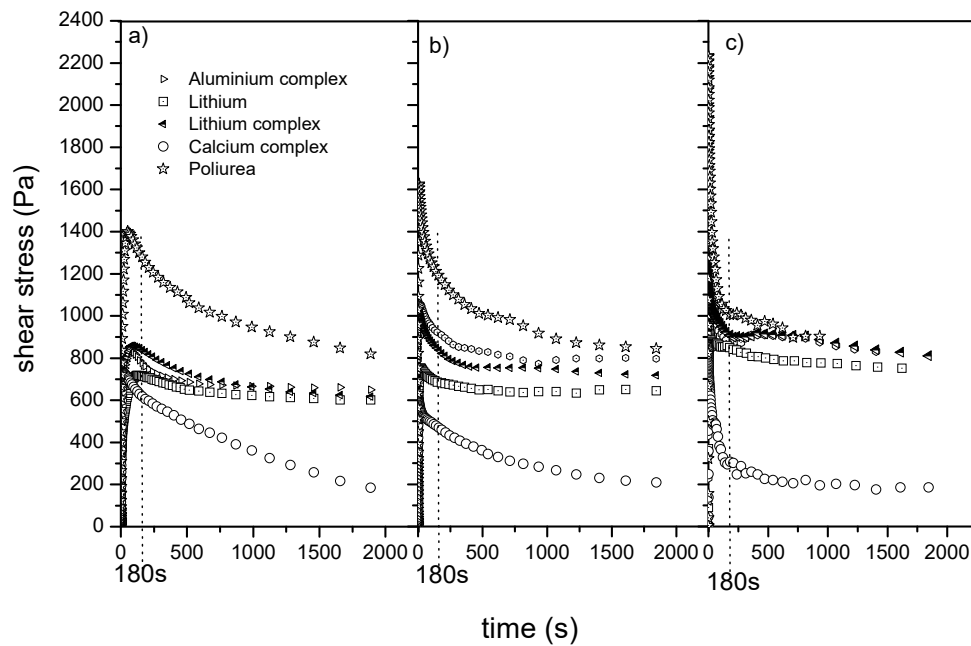


Figure 4. Stress-growth experiments for the greases studied at 0.0125 s^{-1} (a), 0.1 s^{-1} (b), and 1 s^{-1} (c).

As can be appreciated in Figure 4, polyurea-based grease displays the highest values of stress overshoot, as a result of a larger mechanical resistance to flow. This fact is in agreement with the almost parallel trend observed between the storage and loss moduli curves at low frequencies, characteristic of stronger gel-like properties [7,22]. Moreover, both calcium complex and polyurea greases exhibit higher differences between the stress overshoot and the steady-state shear stress, for all the shear rates applied. This fact evidences the important shear-induced structural breakdown occurring in these greases, which can be evaluated by means of the amount of overshoot, defined as follows:

$$S^+ = \frac{\tau_{\max} - \tau_{eq}}{\tau_{eq}} \tag{1}$$

Table 2 shows the values of the amount of overshoot and the elapsed time necessary to reach this overshoot peak (t_{\max}) for the lubricating greases studied, as a function of shear rate. As already mentioned, this time is related to the beginning of the structural breakdown process [35], which decreases with shear rate for all greases.

Table 2. Values of the amount of overshoot (S^+) and time to reach the stress overshoot at different shear rates for all the lubricating greases studied.

Lubricating Greases	0.0125 s^{-1}		0.1 s^{-1}		1 s^{-1}	
	S^+	t_{\max} (s)	S^+	t_{\max} (s)	S^+	t_{\max} (s)
Aluminum Complex	0.282	74	0.321	16.8	0.439	1.91
Lithium	0.172	128	0.157	22.1	0.238	3.08
Lithium complex	0.392	85	0.397	15.7	0.351	1.67
Calcium complex	2.946	26	1.635	2.6	3.043	0.24
Polyurea	0.708	52	0.890	6.8	1.477	0.65

The stress growth curves of lubricating greases have been previously related to shear-induced microstructural changes and associated frictional energy dissipation [36,37]. Thus, the aluminum complex grease, which shows low values of the amount of overshoot and a microstructure based on small dispersed particles (Figure 2a), seems to be relatively stable under low shear rates, similarly to the lithium complex grease, which shows a high density of small fiber-like particles (Figure 2c). The lithium grease shows the highest structural stability against shear, providing the lowest values of the amount of overshoot for all the shear rates applied. These structural features bring about a high level of interactions among soap particles, conferring high elasticity, associated with high t_{\max} values, and consistency, backed up by higher values of the stress overshoot and storage modulus in the entire frequency range studied (Figure 1). On the other hand, although the calcium complex grease shows relatively low values of stress overshoot in comparison with other greases (Figure 4), which must be attributed to its lower NLGI grade, it also shows the most pronounced time-dependent behaviour, with the highest value of the amount of overshoot (Table 2); exhibiting stress overshoot values at least three times higher than the corresponding steady-state value, for each shear rate evaluated (Figure 4). Furthermore, the lowest elapsed time at the overshoot peak (t_{\max}) was detected for this grease. These transient flow properties, followed by those exhibited by the polyurea grease, are a consequence of the lower particle dispersion degree and not so entangled structures like those observed in the case of fibers.

As it has been mentioned above, these transient experiments at a constant shear rate allow us to evaluate the achievement of the steady-state in the previously discussed stepped-ramp flow tests. As can be appreciated in Figure 4, the equilibrium state is reached at 0.0125 and 0.1 s^{-1} much longer than the 3 min applied in the stepped ramps, for all greases. Consequently, the “practical” flow curves displayed in Figure 3 must be significantly corrected in this shear rate range in order to get a more realistic steady-state flow behaviour. On the other hand, fracture, followed by the expulsion of the sample to some extent, was observed when some of the greases were submitted to moderate constant shear rates. This phenomenon hinders the consecution of the final equilibrium stress value. As a consequence, in those cases, the equilibrium time was considered to be reached when a variation of less than 5% of shear stress was maintained for 400 s. Thus, equilibrium times of around 1800, 1400, and 800 s were taken at 0.0125, 0.1, and 1 s^{-1} , respectively, for most of the samples. However, for calcium complex and polyurea greases, variations of up to 19% and 13%, respectively, have to be considered at 0.0125 s^{-1} after 2000 s.

Additionally, creep experiments were also performed. The main benefit of these tests was the relatively low stress values able to be applied, which do not significantly perturb the grease structural skeleton. When the applied shear stress was inferior to the yield stress, an equilibrium time of around eight hours was fixed to reach and effectively verify the steady-state, whereas 4 h allowed us to obtain the steady-state when the applied stress was slightly higher than the yield stress. These equilibrium times were imposed to obtain a variation of the shear rate lower than 2% for at least 300 s.

As can be observed in Figure 5, creep experiments evidence different transient responses, depending on the type of grease. All greases reveal a noticeable jump of the shear rate at a given value of shear stress, which again is indicative of the yielding behaviour of these materials. In addition, it is worth pointing out that for aluminum complex, lithium, and polyurea greases, the shear rate may increase suddenly and sharply from a zero-near value to a high-shear rate value in the same test after a certain shearing time. This fact is appreciated at 700, 490, and 1100 Pa, respectively, which roughly correspond to the apparent yield stress values, i.e., the stress values for which a sudden jump in shear rate was observed in the stepped-stress ramps obtained in the CS mode. Coussot et al. [38] observed a similar phenomenon with a bentonite-water mixture, which was described as “heavy creep instability”. This fact could be associated with the well-known shear banding effect, for which different values of shear rate can coexist for the same shear stress value applied [10,28,31]. Thus, at very low shear stress, the material behaves as a stiff material; however, when grease starts to flow, it seems to do so heterogeneously, and the shear banding phenomenon finally promotes the fracture of the sample.

Figure 6 shows the viscous flow behaviour for the calcium complex grease obtained from the creep test. As can be observed, a quite pronounced drop in viscosity, from 5×10^8 to 3 Pa·s, was noticed when the shear stress was slightly increased from 590 Pa to 595 Pa, i.e., the yield stress. This particularly dramatic drop in viscosity is favored by the relatively weak structural skeleton that, as already discussed, is greatly affected by this critical shear stress value.

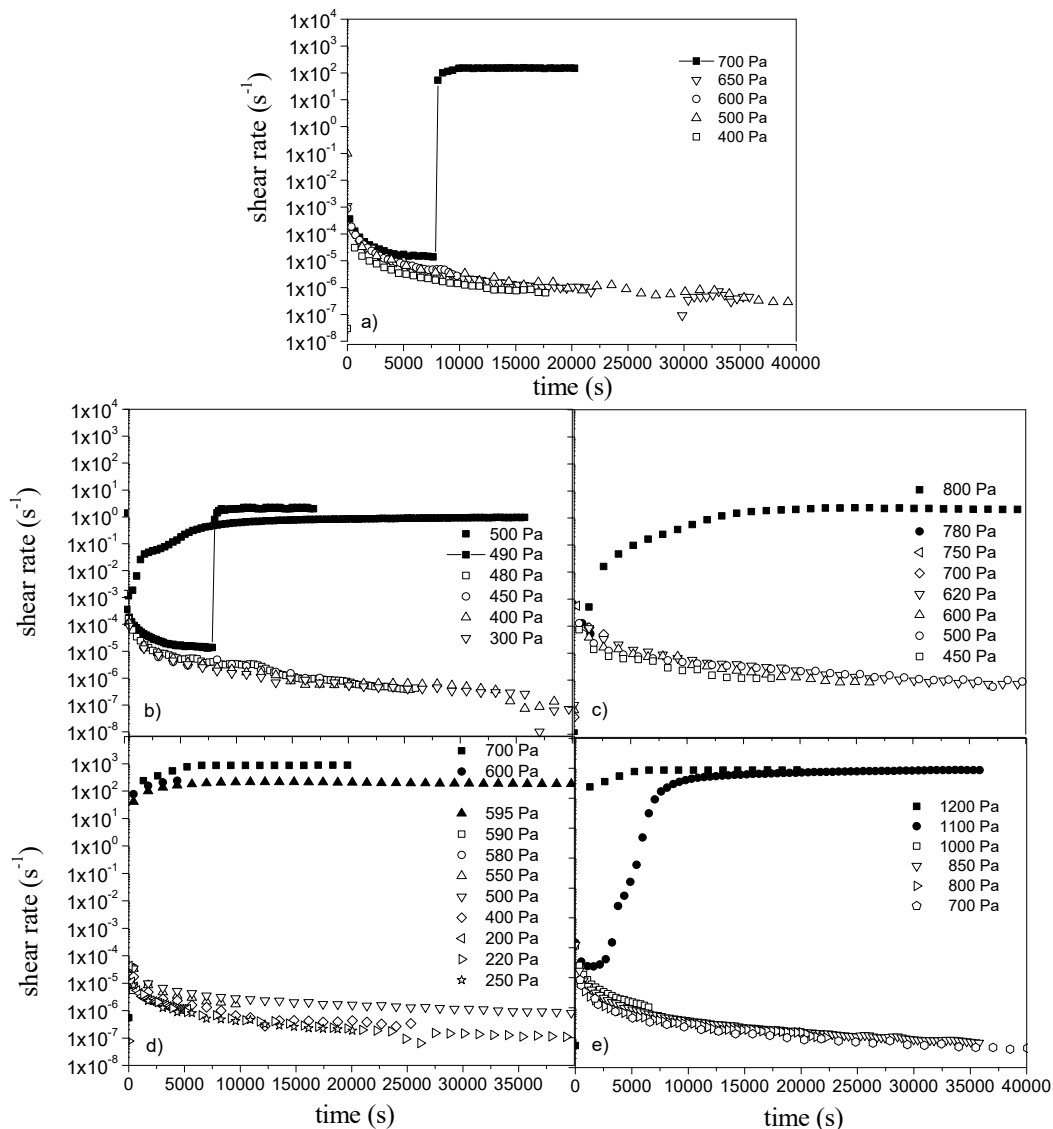


Figure 5. Creep tests for the lubricating greases studied: aluminum complex (a), lithium (b), lithium complex (c), calcium complex (d), and polyurea-based grease (e).

3.4. Correction of the “Practical” Steady-State Flow Curve

Figures 7 and 8 display the correction of the “practical” steady-state flow curves for the five lubricating greases studied, by inserting the equilibrium shear rate/stress values obtained from both creep and stress-growth tests, respectively. The transient stress values at a constant shear rate obtained in stress-growth experiments are not included in Figure 8 because of the difficulty to reach the equilibrium values for both the calcium complex and polyurea greases, as a consequence of the fracture and subsequent partial sample expelling from the measuring gap.

As can be observed in Figures 7 and 8, the non-monotonic evolution observed in stepped-shear rate ramp flow curves was not clearly observed, or significantly dampened, when the equilibrium (or pseudo-equilibrium) stress or shear rate values obtained from stress-growth and creep experiments,

respectively, were plotted. Once again, it must be noticed that the pseudo-equilibrium stress value is that obtained previously for the detection of a significant fracture on samples submitted to a specific constant high shear rate.

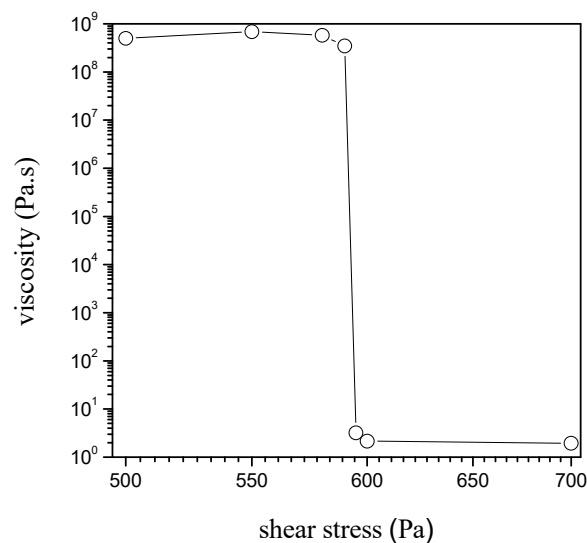


Figure 6. Viscosity vs. shear stress plot obtained from creep tests for the calcium complex grease.

On the other hand and more remarkably, the particularly relevant time-dependent flow behaviour of lubricating greases needs to be considered, especially at low shear rates. Thus, when the shear stress vs. shear rate plots obtained from the stepped-stress or shear rate ramp tests are compared with the equilibrium values obtained from transient experiments, minor correction is necessary for shear rate values higher than 0.1 s^{-1} . However, significant deviations were found below 10^{-3} s^{-1} , as a consequence of the extremely long time required to achieve the steady-state regime at low shear rates or shear stress values. This implies that stress values are noticeably underestimated in stepped-shear rate/stress ramp tests before the yielding flow behavior is apparent (see Figure 3).

Therefore, although stepped-shear rate/stress ramps provide reasonably accurate steady-state data at high shear rates, i.e., above 0.1 s^{-1} for lithium and aluminum greases, long-term experiments are necessary to obtain the steady-state values for lower shear rates and particularly to satisfactorily determine the extension of the yielding region. Overall, the discrepancies of data found in the medium shear rate range, i.e., 10^{-3} – 0.1 s^{-1} , are due to both the time effects already discussed and the non-monotonicity found in the stress evolution, caused by flow instabilities which are favored at shorter times in the stepped shear rate tests, especially in polyurea and calcium greases, but also in the aluminum grease.

In all cases, the Herschel-Bulkley model (Equation (2)) has been used to fit these corrected steady-state flow curves:

$$\tau = \tau_0 + k_H \cdot \dot{\gamma}^n \quad (2)$$

where τ_0 is the yield stress (Pa), k_H is the plastic viscosity ($\text{Pa} \cdot \text{s}^n$), and n is the flow index. These fitting parameters are shown in Table 3.

Table 3. Herschel-Bulkley fitting parameters.

Lubricating Greases	τ_0 (Pa)	k_H (Pa·s ⁿ)	n
Aluminum Complex	654	232	0.28
Lithium	448	301	0.35
Lithium Complex	626	105	0.72
Calcium Complex	543	40	0.15
Polyurea	859	47	0.20

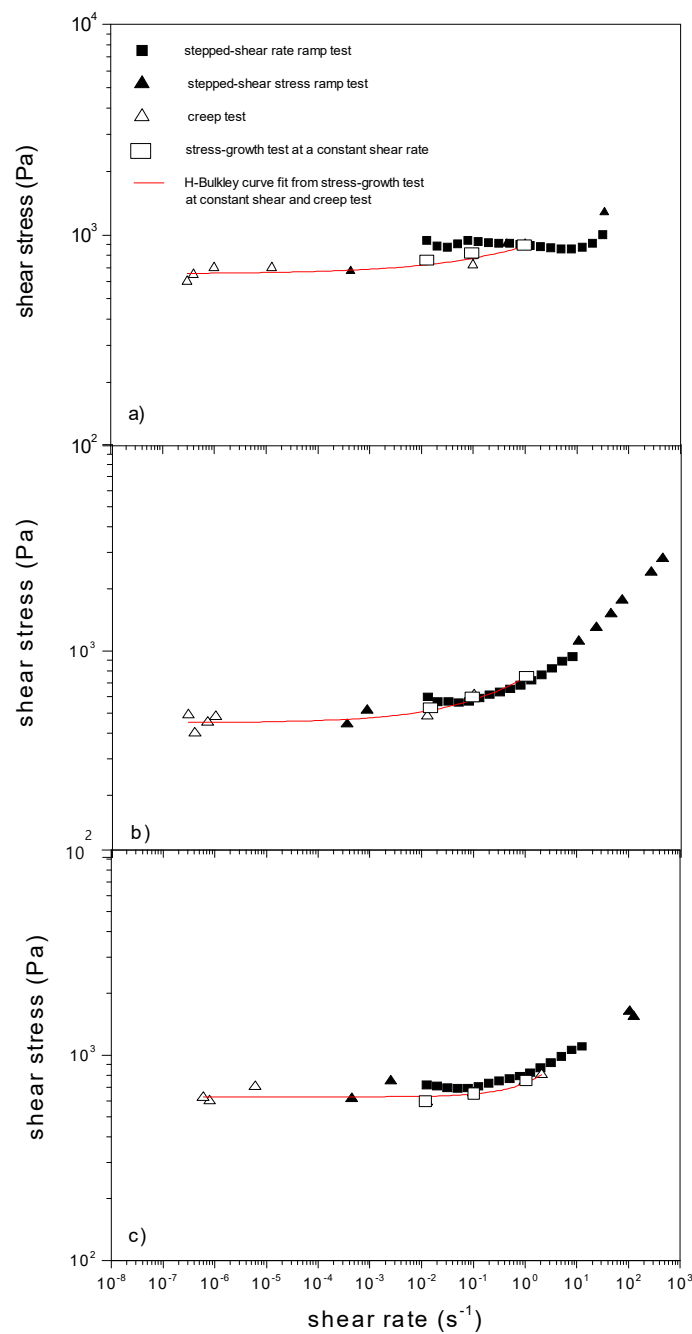


Figure 7. Steady-state flow curves obtained with different rheological tests and fitted to the Herschel-Bulkley model for aluminum complex (a), lithium (b), and lithium complex (c) greases.

As it has been discussed before, the polyurea-based grease exhibits a relatively strong gel-like behaviour in the linear viscoelastic regime and, accordingly, the highest value of τ_0 was obtained for this grease. On the other hand, both calcium complex soap- and polyurea-based greases show the lowest values of the flow index, closely related to the shear-induced structural breakdown [39], which are also in agreement with the values of the amount of overshoot collected in Table 2. In general, lubricating greases with the highest values of the elapsed time at the overshoot reveal the highest values of flow index (Tables 2 and 3). This fact indicates an easier reorientation of the thickener particles in the oily medium, better supporting the shearing action. In consequence, lithium, lithium complex, and aluminum complex greases show a much lower tendency to instabilities during flow.

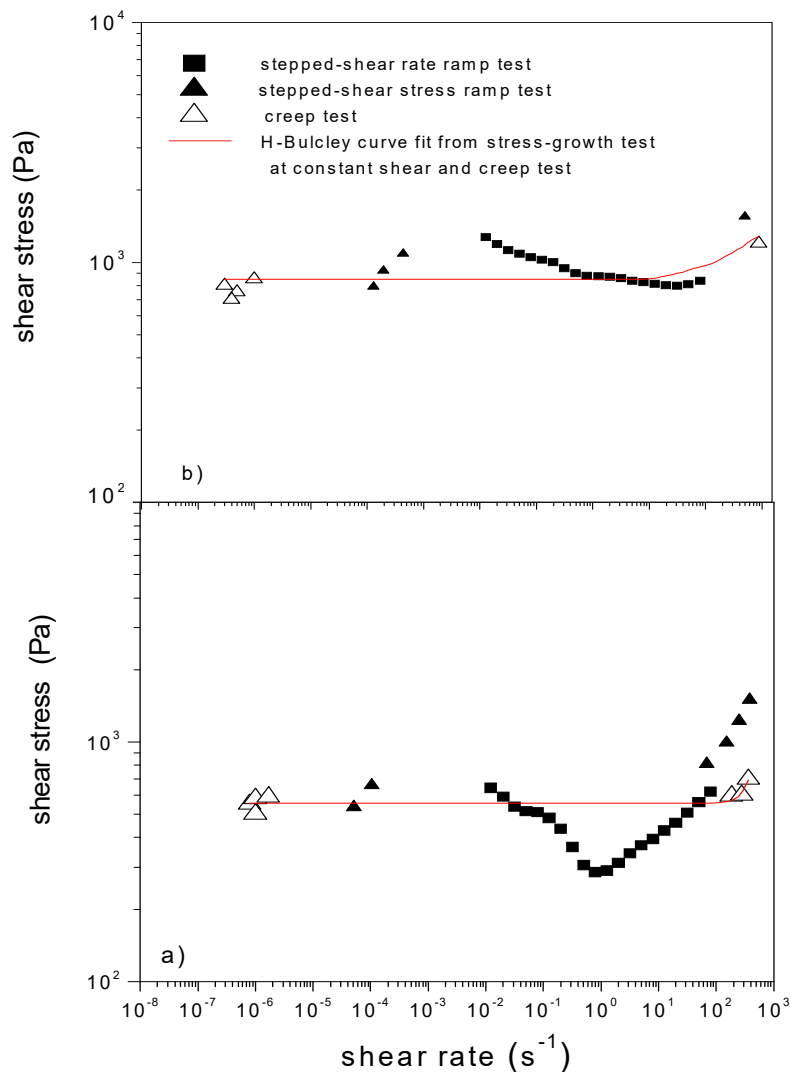


Figure 8. Steady-state flow curves obtained with different rheological tests and fitted to the Herschel-Bulkley model for calcium complex (a) and polyurea (b) greases.

4. Concluding Remarks

Practical viscous flow curves of some lubricating grease formulations evaluated through stepped-shear rate/stress ramp tests exhibit a non-monotonic evolution of shear stress in a wide range of shear rates, which is mainly the consequence of the non-consecution of the steady conditions. In this sense, long-term transient experiments must be conducted to correctly achieve the steady-state for these greases. Transient tests at a constant shear rate are affected by the fracture phenomenon in the shear rate range of $0.0125\text{--}1\text{ s}^{-1}$. Creep experiments make it possible to avoid or minimize

these adverse situations. Both types of transient tests effectively allow the correction of the “practical” flow curves obtained in shear rate/stress-stepped ramps, noticeably dampening the non-monotonic evolution of the stress in the yielding region when considering the real equilibrium stresses or shear rates. These findings may contribute to better understanding the grease flow dynamics in real situations (bearings, seals, ducts, . . .). On one hand, the suitable rheological evaluation of the steady-state flow is necessary to deduce accurate values of rheological parameters, like those of the commonly employed Herschel-Bulkley model, to be used in simulations. On the other hand, the strong effect of time to achieve the steady-state viscosity values and the correct extension of the yielding flow regime must be incorporated in more complex analytical models in order to predict and/or simulated the grease fluid dynamics in practical situations like those described in recent literature [11–17].

Regarding the composition of greases, in spite of the same NLGI grade (except for the calcium complex grease), important differences between them have been detected from both rheological and microstructural points of view, which differentiate these greases in terms of applications and performance levels. Under the same test conditions, while aluminum complex, lithium complex, and lithium greases exhibit the actual flow behaviour of yielding structured materials, calcium complex and polyurea greases show a clearly apparent minimum in the shear stress vs. shear rate plots. Moreover, both of them exhibit the higher values of amount of overshoot in the entire studied shear rate range. Indeed, the calcium complex grease displays a weaker and not so interconnected structure composed of polydisperse and large particle aggregates, which entails a certain brittle character. This fact justifies the highest relative elasticity in the linear viscoelasticity regime and the dramatic drop in viscosity when the yield stress is reached, characterized by the lowest values of the flow index. On the other hand, the low values of the amount of overshoot and the high values of the elapsed time at the overshoot, together with the highest values of the flow index, reveal that lithium and lithium complex greases have the highest structural stability against shearing. In fact, the fiber-like structural units confer a high level of interactions to these greases, without detriment to the easier reorientation of the soap particles in the oil medium, better supporting the shearing action. Finally, it is worth pointing out the stronger gel-like behavior exhibited by the polyurea-based grease in the linear viscoelasticity regime, which confers to this grease the highest values of the yield stress under steady conditions and stress overshoot in transient experiments. Overall, lubricating greases display a complex yielding steady-state flow behaviour, strong time dependence, and associated flow instability effects, which depend on the microstructural characteristics.

Author Contributions: Conceptualization, M.A.D. and J.M.F.; Methodology, S.S. and C.V.; Formal Analysis, M.A.D., S.S. and C.V.; Investigation, M.A.D., S.S., C.V. and J.M.F.; Writing—Original Draft Preparation, M.A.D. and J.M.F.; Writing—Review & Editing, M.A.D. and J.M.F.; Supervision, J.M.F.

Funding: This research received no external funding.

Acknowledgments: Authors gratefully acknowledge Total (France) for kindly providing commercial grease samples.

Conflicts of Interest: The authors declare no conflicts of interest.

References

1. Dawtray, S. Lubricating greases. In *Modern Petroleum Technology*; Hobson, G.D., Pohl, W., Eds.; Applied Science: Essex, UK, 1975.
2. NLGI. *Lubricating Greases Guide*; National Lubricating Grease Institute: Kansas City, MO, USA, 1994.
3. Gow, G. Lubricating grease. In *Chemistry and Technology of Lubricants*, 2nd ed.; Mortier, R.M., Orszulik, S.T., Eds.; Blackie Academic & Professional: London, UK, 1997; pp. 306–319.
4. Mas, R.; Magnin, A. Rheology of colloidal suspensions: Case of Lubricating Greases. *J. Rheol.* **1994**, *38*, 889–908. [[CrossRef](#)]
5. Cho, Y.I.; Choi, E.; Kirkland, W.H. The rheology and hydrodynamic analysis of grease flows in a circular pipe. *Tribol. Trans.* **1993**, *36*, 545–554. [[CrossRef](#)]
6. Delgado, M.A.; Valencia, C.; Sánchez, M.C.; Franco, J.M.; Gallegos, C. Thermorheological behaviour of a lithium lubricating grease. *Tribol. Lett.* **2006**, *23*, 47–54. [[CrossRef](#)]

7. Bondi, A. Theory and Applications. In *Rheology*, 3rd ed.; Eirich, F.R., Ed.; Academic Press: New York, NY, USA, 1960; p. 443.
8. Madiedo, J.M.; Franco, J.M.; Valencia, C.; Gallegos, C. Modeling of the nonlinear rheological behavior of lubricating grease at low shear rates. *J. Tribol.* **2000**, *122*, 590–596. [[CrossRef](#)]
9. Yeong, S.K.; Luckhama, P.F.; Tadros, T.F. Steady flow and viscoelastic properties of lubricating grease containing various thickener concentration. *J. Colloid Interface Sci.* **2004**, *274*, 285–293. [[CrossRef](#)] [[PubMed](#)]
10. Balan, C.; Franco, J.M. Influence of the geometry on the rotational rheometry of lubricating greases. In *The Rheology of Lubricating Greases*; Balan, C., Ed.; ELGI: Amsterdam, The Netherlands, 2000; pp. 43–66.
11. Westerberg, L.G.; Sarkar, C.; Farre-Lladós, J.; Lundstrom, T.S.; Hoglund, E. Lubricating grease flow in a double restriction seal geometry: A computational fluid dynamics approach. *Tribol. Lett.* **2017**, *65*, 82. [[CrossRef](#)]
12. Westerberg, L.G.; Farre-Lladós, J.; Sarkar, C.; Casals-Terre, J. Contaminant particle motion in lubricating grease flow: A computational fluid dynamics approach. *Lubricants* **2018**, *6*, 10. [[CrossRef](#)]
13. Yu, R.F.; Li, P.; Chen, W. Study of grease lubricated journal bearing with partial surface texture. *Ind. Lubr. Technol.* **2016**, *68*, 149–157. [[CrossRef](#)]
14. Wu, Z.H.; Xu, Y.Q.; Deng, S.E. Analysis of dynamic characteristics of grease-lubricated tapered roller bearings. *Shock Vib.* **2018**, *2018*, 7183042. [[CrossRef](#)]
15. Sarkar, C.; Westerberg, L.G.; Hoglund, E.; Lundstrom, T.S. Numerical simulations of lubricating grease flow in a rectangular channel with and without restrictions. *Tribol. Trans.* **2018**, *61*, 144–156. [[CrossRef](#)]
16. Dobrowolski, J.D.; Gawlinski, M.; Paszkowski, M.; Westerberg, L.G.; Hoglund, E. Experimental study of lubricating grease flow inside the gap of a labyrinth seal using microparticle image velocimetry. *Tribol. Trans.* **2018**, *61*, 31–40. [[CrossRef](#)]
17. Li, J.X.; Westerberg, L.G.; Hoglund, E.; Lugt, P.M.; Baart, P. Lubricating grease shear flow and boundary layers in a concentric cylinder configuration. *Tribol. Trans.* **2014**, *57*, 1106–1115. [[CrossRef](#)]
18. Cyriac, F.; Lugt, P.M.; Bosman, R. On a new method to determine the yield stress in lubricating grease. *Tribol. Trans.* **2015**, *58*, 1021–1030. [[CrossRef](#)]
19. Cyriac, F.; Lugt, P.M.; Bosman, R. Yield stress and low-temperature start-up torque of lubricating greases. *Tribol. Lett.* **2016**, *63*, 6. [[CrossRef](#)]
20. Møller, P.C.F.; Mewis, J.; Bonn, D. Yield stress and thixotropy: On the difficulty of measuring yield stresses in practice. *Soft Matter* **2006**, *2*, 274–283. [[CrossRef](#)]
21. Barnes, H.A. The Yield Stress—a review or “ $\pi\alpha\nu\tau\alpha\rho\epsilon\iota$ ”—everything flow? *J. Non-Newtonian Fluid Mech.* **1999**, *81*, 133–178. [[CrossRef](#)]
22. Magnin, A.; Piau, J.M. Shear rheometry of fluids with a yield stress. *J. Non-Newtonian Fluid Mech.* **1987**, *23*, 91–106. [[CrossRef](#)]
23. Hartnett, J.P.; Hu, R.Y.Z. The yield stress - an engineering reality. *J. Rheol.* **1989**, *33*, 671–679. [[CrossRef](#)]
24. Almdal, K.; Dyre, J.; Hvidt, S.; Kramer, O. Towards a phenomenological definition of the term “gel”. *Polym. Gels Netw.* **1993**, *1*, 5–17. [[CrossRef](#)]
25. Sánchez, M.C.; Franco, J.M.; Valencia, C.; Gallegos, C.; Urquiola, F.; Urchegui, R. Atomic force microscopy and thermo-rheological characterization of lubricating greases. *Tribol. Lett.* **2011**, *41*, 463–470. [[CrossRef](#)]
26. Delgado, M.A.; Sánchez, M.C.; Valencia, C.; Franco, J.M.; Gallegos, C. Relationship among microstructure, rheology and processing of a lithium lubricating grease. *Chem. Eng. Res. Des.* **2005**, *83*, 1085–1092. [[CrossRef](#)]
27. Coussot, P. Slow flows of yield stress fluids: Yielding liquids or flowing solids? *Rheol. Acta* **2018**, *57*, 1–14. [[CrossRef](#)]
28. Britton, M.M.; Callaghan, P.T. Nuclear magnetic resonance visualization of anomalous flow in cone-and-plate rheometry. *J. Rheol.* **1997**, *41*, 1365. [[CrossRef](#)]
29. Coussot, P.; Nguyen, Q.D.; Huynh, H.T.; Bonn, D. Avalanche behavior in yield stress fluids. *Phys. Rev. Lett.* **2002**, *88*, 175–207. [[CrossRef](#)] [[PubMed](#)]
30. Coussot, P. Yield stress fluid flows: A review of experimental data. *J. Non-Newtonian Fluid Mech.* **2014**, *211*, 31–49. [[CrossRef](#)]
31. Ovarlez, G.; Rodts, S.; Chateau, X.; Coussot, P. Phenomenology and physical origin of shear localization and shear banding in complex fluids. *Rheol. Acta* **2009**, *48*, 831–834. [[CrossRef](#)]

32. Rubio-Hernandez, F.J.; Paez-Flor, N.M.; Velazquez-Navarro, J.F. Why monotonous and non-monotonous steady-flow curves can be obtained with the same non-Newtonian fluid? A single explanation. *Rheol. Acta* **2018**, *57*, 389–396. [[CrossRef](#)]
33. Mewis, J. Thixotropy—A general review. *J. Non-Newtonian Fluid Mech.* **1979**, *6*, 1–20. [[CrossRef](#)]
34. Barnes, H.A. Thixotropy—A review. *J. Non-Newtonian Fluid Mech.* **1997**, *70*, 1–33. [[CrossRef](#)]
35. Delgado, M.A.; Franco, J.M.; Valencia, C.; Kuhn, E.; Gallegos, C. Transient shear flow of model lithium lubricating greases. *Mech. Time-Depend. Mater.* **2009**, *13*, 63–80. [[CrossRef](#)]
36. Papenhuijzen, J.M.P. The role of particle interactions in the rheology of dispersed systems. *Rheol. Acta* **1972**, *11*, 73–88. [[CrossRef](#)]
37. Kuhn, E. Analysis of a grease-lubricated contact from an energy point of view. *Int. J. Mater. Prod. Technol.* **2010**, *38*, 5–15. [[CrossRef](#)]
38. Coussot, P.; Lenov, A.I.; Piau, J.M. Rheology of concentrated dispersed systems in a low molecular weight matrix. *J. Non-Newtonian Fluid Mech.* **1993**, *46*, 179–217. [[CrossRef](#)]
39. Delgado, M.A.; Valencia, C.; Sánchez, M.C.; Franco, J.M.; Gallegos, C. Influence of soap concentration and oil viscosity on the rheology and microstructure of lubricating greases. *Ind. Eng. Chem. Res.* **2006**, *45*, 1902–1910. [[CrossRef](#)]



© 2019 by the authors. Licensee MDPI, Basel, Switzerland. This article is an open access article distributed under the terms and conditions of the Creative Commons Attribution (CC BY) license (<http://creativecommons.org/licenses/by/4.0/>).